Erschienen in: The journal of biological chemistry : JBC ; 288 (2013), 42. - S. 30597-30606

NMR Reveals Double Occupancy of Quinone-type Ligands in the Catalytic Quinone Binding Site of the Na^+-translocating NADH:Quinone Oxidoreductase from *Vibrio cholerae*[*]

Ruslan Nedielkov[‡1,2], **Wojtek Steffen**[§1], **Julia Steuber**[§3], **and Heiko M. Möller**[‡2,4]

From the [‡]*Department of Chemistry, University of Konstanz, 78457 Konstanz, Germany and the* [§]*Department of Microbiology, University of Hohenheim (Stuttgart), 70599 Stuttgart, Germany*

Background: The Na^+-NQR is a respiratory Na^+ pump found in prokaryotes.
Results: The NqrA subunit binds two quinone-type ligands in direct vicinity to each other.
Conclusion: Simultaneous binding of two quinones enhances catalytic efficiency of the final electron transfer step.
Significance: We provide the first direct experimental evidence of simultaneous quinone binding with relevance for the catalytic mechanism.

The sodium ion-translocating NADH:quinone oxidoreductase (Na^+-NQR) from the pathogen *Vibrio cholerae* exploits the free energy liberated during oxidation of NADH with ubiquinone to pump sodium ions across the cytoplasmic membrane. The Na^+-NQR consists of four membrane-bound subunits NqrBCDE and the peripheral NqrF and NqrA subunits. NqrA binds ubiquinone-8 as well as quinones with shorter prenyl chains (ubiquinone-1 and ubiquinone-2). Here we show that the quinone derivative 2,5-dibromo-3-methyl-6-isopropyl-*p*-benzoquinone (DBMIB), a known inhibitor of the bc_1 and b_6f complexes found in mitochondria and chloroplasts, also inhibits quinone reduction by the Na^+-NQR in a mixed inhibition mode. Tryptophan fluorescence quenching and saturation transfer difference NMR experiments in the presence of Na^+-NQR inhibitor (DBMIB or 2-*n*-heptyl-4-hydroxyquinoline *N*-oxide) indicate that two quinone analog ligands are bound simultaneously by the NqrA subunit with very similar interaction constants as observed with the holoenzyme complex. We conclude that the catalytic site of quinone reduction is located on NqrA. The two ligands bind to an extended binding pocket in direct vicinity to each other as demonstrated by interligand Overhauser effects between ubiquinone-1 and DBMIB or 2-*n*-heptyl-4-hydroxyquinoline *N*-oxide, respectively. We propose that a similar spatially close arrangement of the native quinone substrates is also operational *in vivo*, enhancing the catalytic efficiency during the final electron transfer steps in the Na^+-NQR.

Vibrio cholerae is a marine-borne pathogen causing in 3–5 million disease cases an estimated 100,000–130,000 deaths per year (World Health Organization, 2010). This pathogen, like many other bacteria, harbors a unique respiratory enzyme complex, namely the sodium ion-translocating NADH:quinone oxidoreductase (Na^+-NQR),[5] that is unrelated to the eukaryotic complex I on the level of primary structure yet serves a similar purpose in that it generates an electrochemical gradient across the cytoplasmic membrane that in turn drives many other cellular processes like H^+/Na^+-antiporters, solute uptake, and rotation of the flagellum (1).

Na^+-NQR is composed of six subunits NqrA–F and harbors at least five redox-active cofactors: a non-covalently bound FAD and a 2Fe-2S cluster in the NqrF subunit, two covalently bound FMNs in subunits NqrB und NqrC, and one non-covalently bound riboflavin in the subunit NqrB (2–5). Upon oxidation of NADH, electrons are transferred from NADH via FAD and the 2Fe-2S cluster on NqrF to FMN on NqrC, to FMN on NqrB, and finally to riboflavin on NqrB (6, 7). However, the final step of the reaction cycle, the reduction of the quinone substrate, and the coupling of redox chemistry to sodium ion translocation are still largely unclear.

Already in 1992 it was recognized that the resistance of *Vibrio alginolyticus* toward korormicin, a putative quinone analog, is brought about by two mutations in the NqrB subunit of its Na^+-NQR (8). Therefore, it was expected that the NqrB subunit would carry the active site for quinone binding and reduction. Instead, we have recently identified the NqrA subunit to bind ubiquinone-8 and to interact with short chain quinones in the context of the membrane-embedded/detergent-solubilized holo-Na^+-NQR enzyme complex as well as with the isolated, soluble NqrA subunit (9). On the other hand, Juárez *et al.* (10) have shown that the point mutations at glycine 140 and glycine 141 of the NqrB subunit affect Na^+-NQR reduction activity, leading them to conclude that NqrB would harbor the binding site for ubiquinone-1 (Q_1).

[*] This work was supported in part by contract research of the Baden-Württemberg Stiftung, Forschungsprogramm P-LS-Meth/4 (to J. S. and H. M. M.), and Deutsche Forschungsgemeinschaft Grant FR 1321/3-1 (to J. S.).

[1] Both authors contributed equally to this work.

[2] Supported by the Young Scholar Fund and the Research School Chemical Biology of the University of Konstanz.

[3] To whom correspondence may be addressed. Tel.: 49-711-459-22228; Fax: 49-711-459-22238; E-mail: julia.steuber@uni-hohenheim.de.

[4] To whom correspondence may be addressed. Tel.: 49-7531-88-5174; Fax: 49-7531-88-5149; E-mail: heiko.moeller@uni-konstanz.de.

[5] The abbreviations used are: Na^+-NQR, sodium ion-translocating NADH:quinone oxidoreductase; DBMIB, 2,5-dibromo-3-methyl-6-isopropyl-*p*-benzoquinone; HQNO, 2-*n*-heptyl-4-hydroxyquinoline *N*-oxide; DDM, *n*-dodecyl β-D-maltoside; Q, ubiquinone; STD, saturation transfer difference; ILOE, interligand Overhauser effect; INPHARMA, interligand NOEs for pharmacophore mapping.

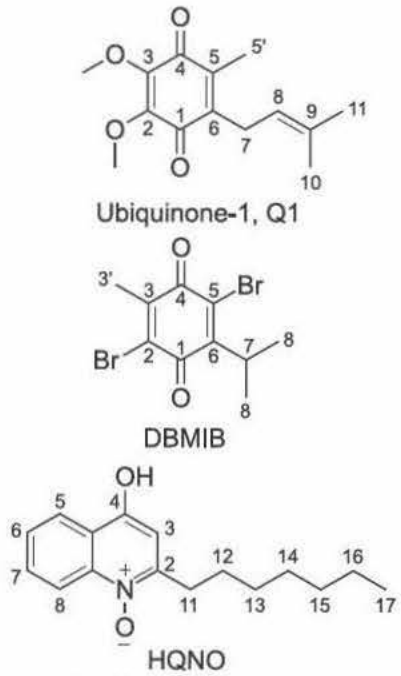

FIGURE 1. **Structures of Q_1, DBMIB, and HQNO including atom numbering.**

The quinone analog 2,5-dibromo-3-methyl-6-isopropyl-*p*-benzoquinone (DBMIB; see Fig. 1) is a potent inhibitor of the mitochondrial bc_1 complex and the cytochrome b_6f complex of chloroplasts (11–15) but can also serve as an electron acceptor with a favorable potential (E_0) of +180 mV (16). The binding of 2 eq of DBMIB into the quinol oxidase (Q_o) pocket of the b_6f complex has been proposed. One equivalent binds with high affinity to a proximal niche, whereas the binding of a second equivalent with low affinity to a distal niche induces a rotation of the Rieske iron-sulfur protein domain of the complex (17). By EPR, it was shown that DBMIB attaches to and modifies the iron-sulfur center in the bc_1 complex with inhibition in the nanomolar range and interacts with cytochrome *b*. A mechanism was proposed whereby DBMIB does not just act as a simple competitor or redox mediator at the quinol oxidase site but also as an antagonist to ubiquinone, inducing a redox bypass of the respiratory chain (18).

Another quinone analog, 2-*n*-heptyl-4-hydroxyquinoline *N*-oxide (HQNO; Fig. 1), was already reported as an inhibitor of the Na^+-NQR from *V. alginolyticus* with a K_I of 0.4 μM (19). In our previous work, we also showed by STD NMR and surface plasmon resonance spectroscopy that HQNO binds to the NqrA subunit (9).

Here we show that DBMIB acts both as an inhibitor and as an alternative substrate of the Na^+-NQR of *V. cholerae* by a specific interaction with the NqrA subunit of the complex. Furthermore, NMR experiments with DBMIB and HQNO indicate that the NqrA subunit possesses an extended binding site for quinone analog ligands that can simultaneously accommodate two quinones involving a high affinity and a low affinity binding mode. Similar dual occupancy models have been proposed for other quinone-converting enzymes based on indirect experimental evidence (20–22). Our findings provide important insight into mechanistic aspects of the final redox step catalyzed by the Na^+-NQR.

EXPERIMENTAL PROCEDURES

Purification of the Na^+-NQR and Subunit NqrA—Full-length Na^+-NQR complex linked to an N-terminal hexahistidine tag on the subunit NqrA was produced and purified as described previously (23). Subunit NqrA encoded on plasmid pBR322 (9) was produced in *Escherichia coli* BL21(DE3). Perdeuterated NqrA was produced in labeled M9 medium according to Marley *et al.* (24). The cells were grown in unlabeled LB medium at 37 °C with shaking at 150 rpm. At an A_{600} of ~0.7, the cells were pelleted by centrifugation for 15 min at 5,000 × *g* at room temperature. The cells were then washed once with M9 medium in D_2O and pelleted again. Cells were resuspended in deuterated M9 medium that was supplemented with perdeuterated glucose and incubated for 1 h at 37 °C and 150 rpm. Subsequently, protein expression was started by addition of isopropyl thio-β-D-galactoside to a concentration of 1 mM. After 4 h of incubation, the cells were harvested. To purify His_6-NqrA, washed cells (25 g) were suspended in 50 mM sodium phosphate, pH 8.0, 300 mM NaCl, 5% (v/v) glycerol. One spatula tip of $MgCl_2$, DNase I (Roche Applied Science), and one tablet of protease inhibitor mixture (Roche Applied Science) were added to the cell suspension, which was passed twice through a French pressure cell at 7.58 megapascals. Cell lysate was centrifuged at 100,000 × *g* for 60 min. The supernatant was filtrated through a syringe filter with a 0.2-μm surfactant-free cellulose acetate membrane (Corning) and loaded onto a HisTrap 2-ml (GE Healthcare) column equilibrated with running buffer (50 mM sodium phosphate, pH 8.0, 300 mM NaCl, 5% (v/v) glycerol, 4 mM NaN_3) containing 20 mM imidazole. NqrA was eluted with running buffer containing 130 mM imidazole. All experiments were performed with monomeric NqrA, which was separated from NqrA aggregates on a Superdex 200 16/60 (GE Healthcare) column in 50 mM phosphate buffer, pH 8.0, 300 mM NaCl, 5% (v/v) glycerol, 4 mM NaN_3 (9).

Enzymatic Assays—NADH dehydrogenase activities of Na^+-NQR were determined with NADH (Applichem) (0.005–0.05 mM) and 0.1 mM Q_1 (MCAT GmbH) at pH 7.5 as described previously (3). Quinone reductase activities were determined with Q_1 (0–0.1 mM) or Q_2 (0–0.1 mM; Sigma-Aldrich) as electron acceptor at a fixed NADH concentration of 50 μM. Rates of NADH oxidation were monitored at 340 nm, and quinol formation was determined from the difference in absorption at 248 and 268 nm (Tables 1 and 2). Kinetic measurements were performed under anaerobic conditions with magnetic stirring on an HP 8452A diode array spectrophotometer (Agilent) in reaction buffer (20 mM Tris-Cl, 50 mM Na_2SO_4, pH 7.5, 0.05 mg/ml BSA (Applichem), 0.05% DDM (Roche Applied Science)) at 25 °C. K_m and V_{max} were calculated using the Michaelis-Menten equation. For enzyme inhibition studies, the Na^+-NQR was incubated at 4 °C in reaction buffer containing DBMIB (Sigma-Aldrich) and Q_1 or Q_2 in <1% ethanol. The reaction was started by adding NADH.

K_I for inhibition of NADH dehydrogenase activity by DBMIB was calculated assuming an uncompetitive mode of inhibition (25). The correlation coefficients and kinetic constants of specific quinone reductase activities are listed in Table 2. The rates were background-corrected by the changes in absorbance aris-

TABLE 1

Inhibition of Na^+-NQR by DBMIB at varying NADH concentrations described by the Michaelis-Menten formalism

The concentration of Q_1 in the assays was 0.1 mM. Both NADH oxidation and quinol formation were recorded. Corresponding rates are presented in Fig. 2. For calculation of K_I', the equation for uncompetitive inhibition was applied: $v_0 = (V_{max}[S])/(K_m + \alpha'[S])$ where $\alpha' = 1 + [I]/K_I'$ (25).

Activity recorded	0 μM DBMIB	10 μM DBMIB
NADH oxidation		
R^2	0.9998	0.9956
V_{max} (μmol min^{-1} mg^{-1})	147.5 ± 1.7	63.1 ± 2.5
K_m (μM)	29.6 ± 0.6	15.1 ± 1.4
K_m/V_{max}	0.2	0.24
K_I' (μM)		7.5
Quinol formation		
R^2	0.9985	0.9904
V_{max} (μmol min^{-1} mg^{-1})	38.9 ± 1.2	19.4 ± 1.0
K_m (μM)	24.5 ± 1.5	12.4 ± 1.7
K_m/V_{max}	0.63	0.64
K_I' (μM)		9.9

TABLE 2

Analysis of the rates of quinol formation by Na^+-NQR at varying Q_1 or Q_2 concentrations in the absence or presence of DBMIB

The NADH concentration in the assays was 50 μM. The rates of Q_1 and Q_2 reduction were background-corrected by the rate of quinol formation when using DBMIB as the sole electron acceptor as shown in the bottom section of the table. For calculation of K_I and K_I', the equation for mixed inhibition was applied: $v_0 = (V_{max}[S])/(\alpha K_m + \alpha'[S])$ where $\alpha = 1 + [I]/K_I$ and $\alpha' = 1 + [I]/K_I'$ (25).

Q_1 reductase			
Michaelis-Menten formalism		10 μM	25 μM
$v_0 = (V_{max} * [S]) / (K_M + [S])$	No DBMIB	DBMIB	DBMIB
R^2	0.9963	0.9811	0.9874
V_{max} [μmol min^{-1} mg^{-1}]	25.8 ± 0.6	22.6 ± 1.4	15.2 ± 1.1
K_M [μM]	14.0 ± 0.9	19.4 ± 3.1	39.5 ± 6.0
K_I [μM]		35.9	38.7
K_I' [μM]		70.6	35.8
Q_2 reductase			
Boltzmann formalism			25 μM
$y = A2 + (A1\text{-}A2)/(1 + e^{((x-x0)/dx)})$	No DBMIB		DBMIB
R^2	0.9954		0.9917
A1 [μmol min^{-1} mg^{-1}]	-0.6 ± 1.3		-7.5 ± 4.5
A2 [μmol min^{-1} mg^{-1}]	38.9 ± 0.7		28.8 ± 0.7
x0 [μM]	15.0 ± 0.5		9.5 ± 2.6
dx[μM]	3.6 ± 0.4		7.0 ± 1.1
DBMIB reductase			
Michaelis-Menten formalism			
$v_0 = (V_{max} * [S]) / (K_M + [S])$	No Q		
R^2	0.9944		
V_{max} [μmol min^{-1} mg^{-1}]	5.6 ± 0.3		
K_M [μM]	53.7 ± 6.3		

TABLE 3

Dependence of STD NMR effects of Q_1 on the concentration of DBMIB in the presence of NqrA and Na^+-NQR, respectively, and on the concentration of HQNO in the presence of NqrA

Changes of STD effects shown in Figs. 5–7 were globally fitted to a one-site binding model: $\Delta I_{STD} = \Delta I_{STD,max} \times c_{ligand}/(k + c_{ligand})$.

	NqrA/Q_1/DBMIB	Na^+-NQR/Q_1/DBMIB	NqrA/Q_1/HQNO
R^2	0.97	0.83	0.89
k	26.69 ± 2.59	28.52 ± 11.18	50.97 ± 8.69

ing from DBMIB reduction by the Na^+-NQR to enable kinetic analysis of ubiquinol formation only. The reductase activity of Na^+-NQR using only DBMIB as electron acceptor (16) was assayed under identical conditions as Q_1 reductase activity with DBMIB concentrations between 0 and 100 μM using the same extinction coefficient as for Q_1 (Table 2).

Binding of DBMIB Determined by Tryptophan Fluorescence Spectroscopy—NqrA was diluted in 50 mM phosphate buffer, 300 mM NaCl, pH 8.0, 5% (v/v) glycerol to a concentration of 1 μM. DBMIB was added from an ethanol stock solution to final concentrations between 0 and 200 μM (final ethanol concentration, 1%). Fluorescence was analyzed with a Fluorolog 3 spectrofluorometer (Horiba Scientific) using a temperature-controlled quartz cuvette. Measurements were performed in triplicate at 10 °C. The intensity of tryptophan fluorescence emission was determined at 338 nm ($\lambda_{excitation}$ = 295 nm). The increase in quenching (ΔF) of the tryptophan emission was normalized to values between 0 and 1 and plotted against the concentration of DBMIB. Non-linear regression analyses were performed using the equations for one-site binding and two-site binding in Origin 6.1.

NMR Spectroscopy—NqrA was transferred to D_2O containing 10 mM potassium phosphate, pH 8.0, 150 mM NaCl, 4 mM NaN_3 (PBS buffer) by repeated (at least 5-fold) ultrafiltration with Ultrafree 4 membranes (Millipore; molecular mass cutoff, 10 kDa). Na^+-NQR was transferred to the same buffer as used for NqrA with addition of 0.05% DDM; Ultrafree 4 membranes with molecular mass cutoff of 100 kDa were used in this case. To 10 μM NqrA or Na^+-NQR, respectively, Q_1 was added from 20 mM stock solutions in DMSO-d_6 to a final concentration of 100 μM. DBMIB and HQNO were added from 20, 4, or 1 mM stock solutions in DMSO-d_6 to obtain NqrA samples containing 0, 5, 10, 20, 40, 60, 80, 100, 125, or 150 μM DBMIB or HQNO, respectively, and additionally 200 μM in the case of HQNO. Additional DMSO-d_6 was added to keep its concentration constant within the series (1.5%, v/v). The STD NMR experiment with DBMIB alone was performed with 2.5 μM NqrA in PBS buffer. DBMIB was added from a 20 mM stock solution to a concentration of 100 μM. Controls were prepared in the same way without NqrA. The samples were transferred to 5-mm NMR tubes, and STD NMR experiments (26) were performed as described (9). The resonances of Q_1 were assigned as described (9). Water suppression was achieved by excitation sculpting (27). Resonances of NqrA and Na^+-NQR, respectively, were saturated by applying a train of low power Gaussian-shaped pulses at 0.2 ppm with a total saturation time of 2 s. Off-resonance irradiation was set to 33 ppm. Under these conditions, percent STD in control experiments was below 3% for the most upfield methyl group of DBMIB (H-8) and below 1% for all other protons. On- and off-resonance spectra were acquired in an interleaved manner and subtracted after processing. Up to 4096 transients were collected at a spectral width of 12 ppm. Percent STD effects were determined within the multiple display mode by scaling the off-resonance spectrum down to superimpose with the signal of interest in the difference (off − on) spectrum. The influence of DBMIB or HQNO, respectively, on Q_1 STD effects was plotted in Origin 8.1G and fitted to a one-site binding model equation: $y = \Delta I_{STD,max} \times x/(k + x)$. One value for k was obtained from globally fitting all Q_1 signals (Table 3).

Experiments for detecting interligand Overhauser effects (ILOEs) were performed in the same buffer as STD NMR experiments. To 25 μM NqrA or perdeuterated NqrA (prepared as described above), respectively, 200 μM Q_1 and 400 μM DBMIB or HQNO were added from 20 mM stock solutions in DMSO-

d_6. DMSO-d_6 was added to a final concentration of 5% in the sample. Two samples for control experiments were prepared in the same manner but excluding NqrA or quinone analogs, respectively. The two-dimensional NOESY experiments were performed with water suppression achieved by low power presaturation of the water signal during relaxation delay and mixing time (28, 29). The mixing time was set to 600 ms. Up to 1024 increments with 48 scans in each increment were collected at a spectral width of 10 ppm. Selective one-dimensional NOESY experiments based on the double pulsed field gradient spin-echo method were performed using Bruker's pulse program SELNOGP (30). Resonances of interest were selectively excited with a low power Gaussian-shaped pulse. The mixing time was set to 600 ms. Up to 8192 scans were collected at a spectral width of 20 ppm.

All NMR experiments were acquired at 300 K on a Bruker AVANCE III 600-MHz spectrometer equipped with a cryogenic 5-mm TCI-H/C/N triple resonance probe with actively shielded z-gradient. Spectra were processed and analyzed with the software TopSpin (Bruker; v3.1).

RESULTS

Interaction of Na^+-NQR with Q_1 and DBMIB Monitored by the Electron Transfer Activities—As DBMIB is an analog and antagonist of ubiquinone, it was used in this work to obtain information on quinone binding by the Na^+-NQR. First, we questioned whether DBMIB has an influence on NADH oxidation by the Na^+-NQR. The effect of DBMIB on NADH oxidase activity was assayed by maintaining a constant concentration of the artificial electron acceptor Q_1 while varying the concentration of the substrate NADH. Both NADH oxidation and quinol formation rates were recorded. Determined V_{max} and K_m values for NADH oxidase activity were 147.5 ± 1.7 μmol min^{-1} mg^{-1} and 29.6 ± 0.6 μM, respectively, when quantifying NADH oxidation and 38.9 ± 1.2 μmol min^{-1} mg^{-1} and 24.5 ± 1.5 μM, respectively, when analyzing quinol formation (Table 1). The difference between the two rates is caused by reaction of ubisemiquinone with oxygen as described (31). Preincubation of the enzyme with 10 μM DBMIB led to a decrease in the NADH oxidation rate V_{max} as well as in the Michaelis constant K_m with similar manifestations on the NADH oxidation and quinol formation rates (Fig. 2).

Varying the ubiquinone-1 concentration of the buffer while starting the assay always by adding 50 μM NADH allowed for characterization of the quinone reductase activity of the Na^+-NQR. Assays in the absence of DBMIB displayed a clearly defined Michaelis-Menten-like behavior of the enzyme with a V_{max} value of 25.8 ± 0.6 μmol min^{-1} mg^{-1} and a K_m value of 14.0 ± 0.9 μM for quinol formation (Table 2). If quinone reductase activity was measured in the presence of 10 or 25 μM DBMIB (Fig. 3, *upper panel*), a decrease of V_{max} and an increase of K_m values were observed (Table 2).

We also performed enzymatic assays with ubiquinone-2, decylubiquinone, and ubiquinone-10. With Q_2, similar quinol formation rates were observed as with Q_1; however, the measured rates show a sigmoidal dependence on the concentration of Q_2 and did not yield meaningful kinetic parameters (Fig. 3, *lower panel*, and Table 2). This observation is in accordance

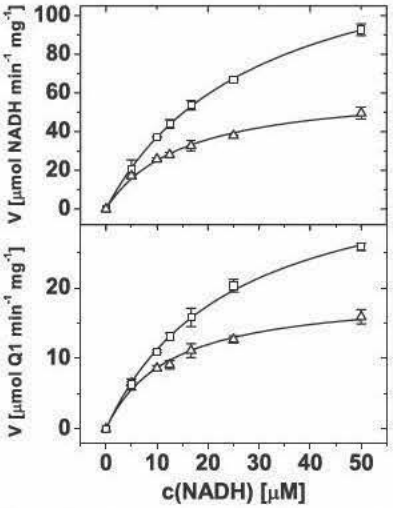

FIGURE 2. **Inhibition of Na^+-NQR by DBMIB determined at varying concentrations of NADH.** Assays were performed in the presence of 0.1 mM Q_1. Specific activities (*V*) are expressed as μmol of NADH used or μmol of QH_2 formed/mg of enzyme/min in the absence (*squares*) or presence of 10 μM DBMIB (*triangles*). Kinetic measurements were performed in triplicate. *Error bars* represent S.D. Kinetic constants are summarized in Table 1. *Upper panel*, NADH oxidation. *Lower panel*, quinol formation.

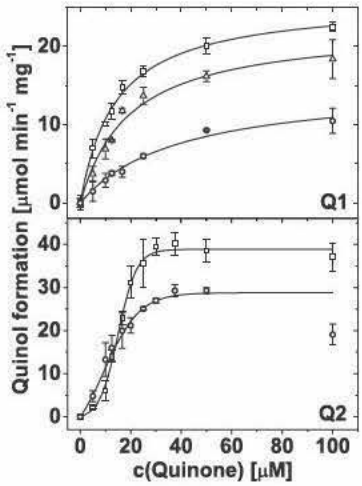

FIGURE 3. **Quinone reductase activities of Na^+-NQR in the presence or absence of DBMIB.** Specific activity is expressed as μmol of Q_1 or Q_2 reduced/mg of enzyme/min. Rates were measured without addition of DBMIB (*squares*) and in the presence of 10 (*triangles*) or 25 μM (circles) DBMIB. The *upper panel* depicts Michaelis-Menten fits of Q_1 reductase activity. Fitting of the Q_2 reductase activity (*lower panel*) to a Michaelis-Menten model resulted in weak correlation ($R^2 < 0.83$); instead sigmoidal fits are presented. Kinetic measurements were performed in triplicate. *Error bars* represent S.D.

with earlier reports (32) and is most likely caused by diffusion and desolvation processes involving the DDM micelle that become rate-limiting under these conditions. In the case of decylubiquinone and Q_{10}, significantly lowered rates compared with Q_1 were observed (data not shown). This precludes inhibition studies with DBMIB because, under these conditions, DBMIB itself will be reduced much faster than decylubiquinone or Q_{10}.

Binding of DBMIB to the NqrA Subunit—We have recently shown that subunit NqrA of the Na^+-NQR harbors a Q binding site (9). We now asked whether NqrA also interacts with DBMIB. NqrA contains three tryptophan residues. Measurement of tryptophan fluorescence during DBMIB titration

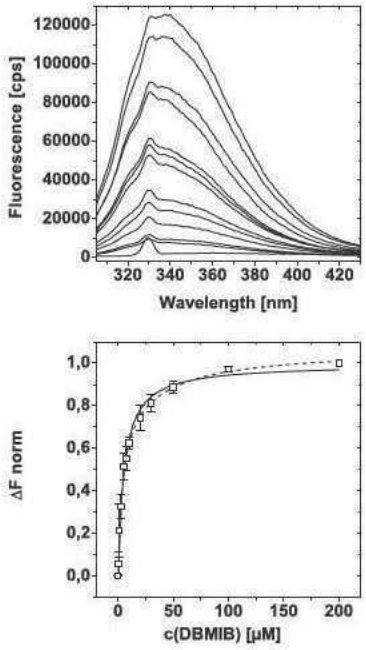

FIGURE 4. **Binding of DBMIB to NqrA monitored by quenching of tryptophan fluorescence.** *Upper panel*, fluorescence emission spectra of, from *top* to *bottom* (using 338 nm as reference), 1 μM NqrA titrated with 0, 0.5, 1, 2.5, 5, 7.5, 10, 20, 30, 50, 100, and 200 μM DBMIB. The *bottom-most* spectrum is buffer only (50 mM Tris-HCl, 300 mM NaCl, pH 8, 5% glycerol). The excitation wavelength was 295 nm. Samples were measured in triplicates; one spectrum of each condition is shown. DBMIB exhibits no fluorescence in the analyzed wavelength range (data not shown). *Lower panel*, the increase in quenching (ΔF) of the tryptophan emission at 338 nm depicted in the *upper panel* was normalized (*norm*) to values between 0 and 1 and plotted against the concentration of DBMIB. Non-linear regression analysis using a one-site binding model (*solid line*) and a two-site binding model (*dashed line*) was performed. *Error bars* represent S.D.

TABLE 4

Binding of DBMIB to the NqrA subunit according to tryptophan fluorescence quenching

Fluorescence data were fitted to a one- or two-site binding model.

One-site binding model:	
$y = B_{max} \times x/(k_1 + x)$	
R^2	0.99135
B_{max}	0.99 ± 0.02
k_1 (μM)	5.42 ± 0.49
Two-site binding model:	
$y = B_{max1} \times x/(k_1 + x) + B_{max2} \times x/(k_2 + x)$	
R^2	0.99645
B_{max1}	0.36 ± 0.17
B_{max2}	0.71 ± 0.20
k_1 (μM)	33.24 ± 34.10
k_2 (μM)	3.08 ± 1.11

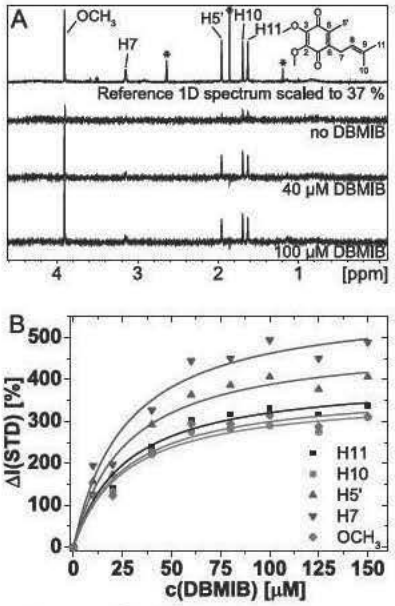

FIGURE 5. **Saturation transfer difference NMR spectroscopy of Q_1 and DBMIB in the presence of NqrA.** *A*, reference (*upper panel*) and three STD NMR (*three lower panels*) spectra of Q_1 at increasing DBMIB concentration in the presence of NqrA. The reference spectrum was scaled to 37% of its original intensity. Signals of the same intensity in the STD spectrum correspond to an STD effect of 37%. The panel shows growing STD effects of Q_1 signals with increasing DBMIB concentration. Impurities and solvent signals are marked with *asterisks*. *1D*, one-dimensional. *B*, changes of saturation transfer difference NMR effects of Q_1 depending on the concentration of DBMIB. Experimental data points were fitted to a one-site binding model ($y = I_{max} \times x/(k + x)$; *solid lines*); the constant *k* was fitted globally for all curves.

enabled us to detect changes in the microenvironment of the binding site. Incubation of NqrA with DBMIB led to quenching of the fluorescence. Saturation of the quenching was observed at concentrations >100 μM DBMIB with 6% of the original fluorescence remaining, indicating that at least two of the three tryptophan residues of the protein are closely affected by DBMIB binding. The data were fitted to one-site and two-site binding models (Fig. 4). The goodness of fit was slightly higher with the two-site model, yielding an apparent K_D value of 3.08 ± 1.11 μM and a second K_D value of 33.24 ± 34.10 μM (Table 4).

As a control, we performed the same titration with Q_1 (data not shown); however, Q_1 is apparently not as well suited for fluorescence quenching studies as DBMIB as documented by fluctuating data points at low concentrations. Therefore, we refer to the K_D values reported previously (9).

STD NMR confirmed the binding of DBMIB to NqrA with, at a given ligand-to-protein-ratio, STD effects that were even stronger (maximum, 25%) than with Q_1 (maximum, 8.5%) (data not shown). Furthermore, signals in the proton NMR spectrum of DBMIB became broad and shifted upon binding to NqrA, which is indicative of a binding kinetic at the intermediate NMR time scale. To circumvent problems caused by exchange, broadening STD effects were quantified at a higher excess of DBMIB (40:1) as compared with experiments with Q_1. The strongest STD signals originated from the isopropyl group of DBMIB (methyl groups, 25.0%; CH group, 24–25%). The methyl group bound directly to the quinone ring showed an STD effect of 16.1%. This suggests that the isopropyl group of DBMIB is in closest contact to NqrA.

The Inhibitor DBMIB and Ubiquinone Q_1 Bind Simultaneously to the NqrA Subunit as Well as to Holo-Na^+-NQR—To investigate how DBMIB affects the binding of Q_1 to the Na^+-NQR, we studied the influence of DBMIB on the STD effects of Q_1 at constant Q_1 concentration with holo-Na^+-NQR and the NqrA subunit, respectively (Figs. 5 and 6). To this end, STD effects in the absence of DBMIB were set as a reference, and all other effects measured in the presence of the inhibitor were expressed as percent changes. Importantly, STD effects increased with higher concentrations of DBMIB in the presence of Na^+-NQR as well as NqrA. STD effects of Q_1 were affected by DBMIB in a concentration-dependent fashion. This effect

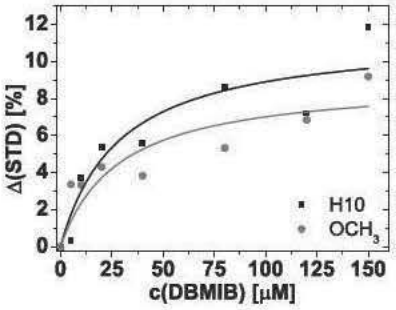

FIGURE 6. **Saturation transfer difference NMR spectroscopy of Q_1 and DBMIB in the presence of Na^+-NQR.** Changes of saturation transfer difference NMR effects of Q_1 depending on the concentration of DBMIB are shown. Experimental data points were fitted to a one-site binding model ($y = I_{max} \times x/(k + x)$; *solid lines*); the constant k was fitted globally for both curves.

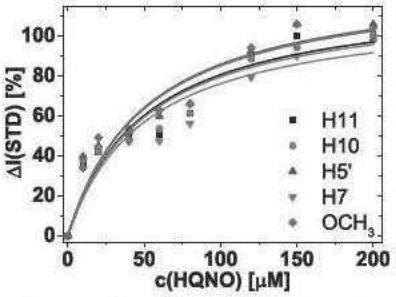

FIGURE 7. **Saturation transfer difference NMR spectroscopy of Q_1 and HQNO in the presence of NqrA.** Changes of saturation transfer difference NMR effects of Q_1 depending on the concentration of HQNO are shown. As with DBMIB, experimental data points were fitted to a one-site binding model ($y = I_{max} \times x/(k + x)$; *solid lines*); the constant k was fitted globally for all curves.

leveled off at DBMIB concentrations above 80–100 μM in both cases. STD changes of signals of Q_1 were fitted globally to a one-site binding model ($y = \Delta I_{STD,max} \times x/(k + x)$). All five signals of Q_1 were used in the case of NqrA, and two signals of Q_1 could be quantified reliably in the case of Na^+-NQR. The other signals were occluded by DDM or affected by spectral artifacts. Resulting EC_{50} values (k) were 28.5 ± 11.2 μM for the Na^+-NQR and 26.7 ± 2.6 μM for NqrA (Table 3). It should be noted that determining changes of STD effects cannot be performed with highest accuracy because of the intrinsically low signal-to-noise ratio. Therefore, the EC_{50} values obtained by this technique should be considered as estimates with error margins in the range of 10–30% in the present case.

An identical experiment was also done with Q_1 and HQNO in the presence of NqrA. The influence of HQNO on STD effects of Q_1 was very similar to the influence of DBMIB (Fig. 7). STD changes of signals of Q_1 were fitted globally to a one-site binding model ($y = \Delta I_{STD,max} \times x/(k + x)$), which provided an EC_{50} value of 51.0 ± 8.7 μM (Table 3).

The influence of DBMIB on STD effects of Q_1 was also analyzed with regard to the binding mode of Q_1 (Table 5). For this purpose, a ratio between the STD effect of Q_1 at maximal concentration of DBMIB and in the absence of DBMIB was calculated. These ratios were then normalized to the minimal ratio (for H-10) that was set to 1. Rather than increasing or decreasing all STD effects of Q_1 homogeneously, the quinone analog DBMIB affected the STD intensities of H-5′ and H-7 more strongly than the remaining signals of Q_1. Our analysis shows that STD effects of H-5′ and H-7 increased disproportionately

TABLE 5
Relative changes of the STD effects of Q_1 induced by the presence of DBMIB

Signal	STD effects of Q_1: No DBMIB	STD effects of Q_1: 150 μM DBMIB	Ratio 150 μM/0 μM DBMIB	Relative ratio (ratio(H-10) = 1)
	%			
H-11	6.0	26.3	4.38	1.07
H-10	7.5	30.7	4.09	1.00
H-5′	5.1	25.8	5.06	1.24
H-7	3.4	20.0	5.88	1.44
OCH_3	8.5	34.9	4.11	1.00

upon addition of DBMIB, suggesting that these protons are brought into closer contact to the binding site in the presence of the inhibitor.

The Inhibitors DBMIB and HQNO and Ubiquinone Q_1 Occupy an Extended Quinone Binding Site—The fact that, according to STD NMR, DBMIB and HQNO, respectively, do not displace Q_1 from the binding site but alter the binding mode of the native substrate led us to surmise whether both pairs, Q_1/DBMIB and Q_1/HQNO, interact with NqrA in direct vicinity to each other.

To test this, we recorded NOESY spectra of both pairs of ligands in the presence of NqrA (Figs. 8 and 9). Indeed, we observed ILOEs between Q_1 and DBMIB and between Q_1 and HQNO (33). These correlations were only observed in the presence of NqrA. A mixture of both ligands in the absence of NqrA did not show ILOEs (Figs. 8 and 9) nor did NqrA show cross-peaks at these positions in the absence of ligands. It is important to note that the observation of ILOEs critically depends on the presence of NqrA yet proved independent of whether protonated or perdeuterated NqrA was used during NOESY experiments (Fig. 8). This would indicate that the correlations observed originate from direct transfers between the ligands and not from protein-mediated effects.

Further evidence for a critical role of NqrA for observing ILOEs is that, in the absence of NqrA, Q_1 and DBMIB did not mutually perturb their chemical shifts. This indicates that both quinone analogs do not form complexes in solution.

DISCUSSION

The kinetic characterization of the Na^+-NQR complex suggests that quinone reduction is best described by the classic Michaelis-Menten formalism, indicating a single catalytically active quinone binding site. However, our recent surface plasmon resonance study of Q_1 binding to the isolated NqrA subunit provided hints for the presence of a second quinone binding site with lower affinity (9). Furthermore, numerous studies report uncompetitive inhibition of the Na^+-NQR by inhibitor molecules that are supposed to interact with the quinone binding site (8, 34). It is also noteworthy that enzyme complexes catalyzing related chemical reactions (bc_1 complex and b_6f complex) were indirectly shown to have spacious quinone binding sites that can accommodate more than 1 quinone eq at a time at least according to inhibitor studies by high resolution magic angle spinning NMR spectroscopy (21) and according to EPR experiments (20, 22).

Most recently, crystal structures of the alternative NADH dehydrogenase Ndi1 from yeast were reported (35, 36). Indeed,

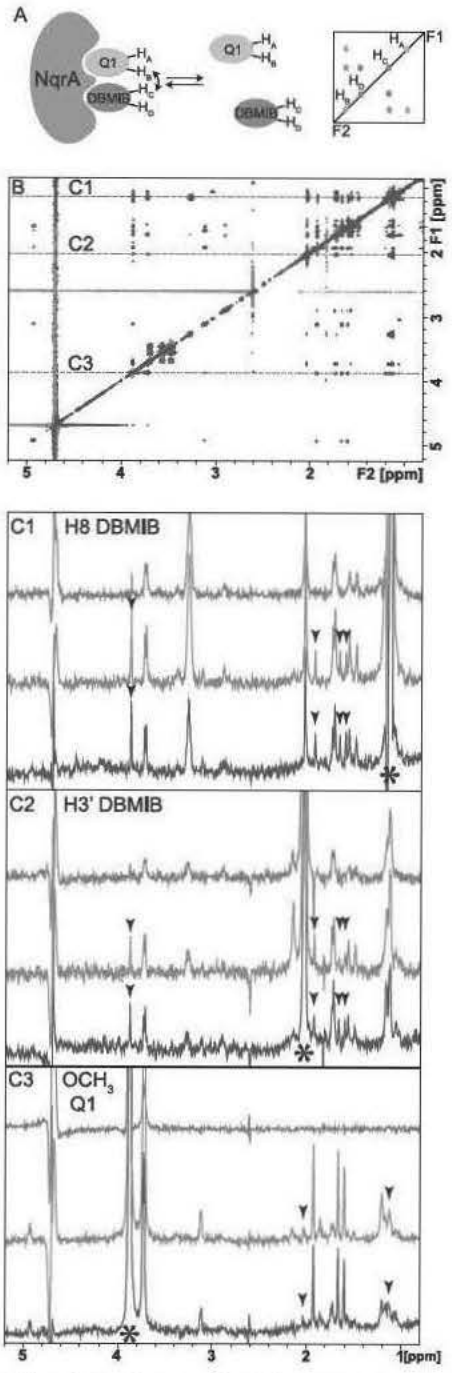

FIGURE 8. **Interligand Overhauser effects between Q_1 and DBMIB in the presence of NqrA.** *A*, scheme illustrating the buildup of an intermolecular NOE due to simultaneous binding of both ligands in direct vicinity to each other within the receptor binding site. *B*, expansion of the NOESY spectrum of 200 μM Q_1 and 400 μM DBMIB in the presence of 25 μM NqrA in deuterated PBS buffer (150 mM NaCl, 10 mM NaP_i, 4 mM NaN_3 in D_2O). The mixing time was 600 ms. Chemical shifts at which traces were extracted for *C1–C3* are indicated by *dashed lines*. *C*, three panels (*C1*, *C2*, and *C3*) showing traces extracted from the NOESY spectrum of Q_1 and DBMIB. The ligand atom giving rise to the diagonal signal is indicated at the *top left* of each panel, and the diagonal signal is marked with an *asterisk*. In each panel, the *blue* trace originates from the NOESY spectrum measured in the presence of protonated NqrA, the *green* trace was measured in the presence of perdeuterated NqrA, and the *red* trace was measured in the absence of NqrA. ILOEs are indicated by *arrowheads*. The position of the diagonal signal is marked with an *asterisk*.

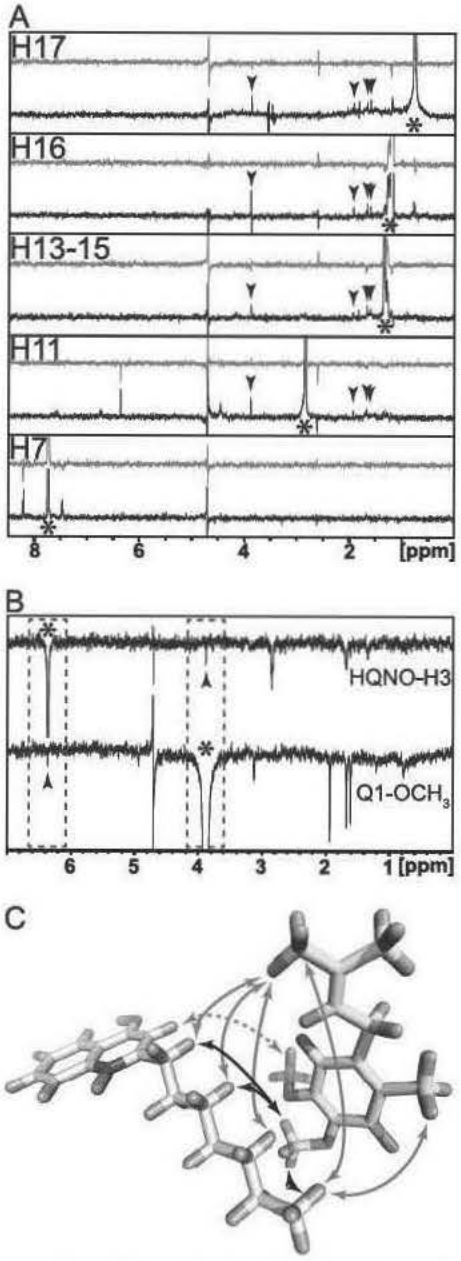

FIGURE 9. **Interligand Overhauser effects between Q_1 and HQNO in the presence of NqrA.** *A*, five panels showing traces extracted from the NOESY spectrum of 200 μM Q_1 and 400 μM HQNO in the presence of 25 μM NqrA in deuterated PBS buffer (150 mM NaCl, 10 mM NaP_i, 4 mM NaN_3 in D_2O). In each panel, the *black* trace originates from the NOESY spectrum measured in the presence of protonated NqrA, and the *red* trace was measured in the absence of NqrA. ILOEs are indicated by *arrowheads*. The position of the diagonal signal is marked with an *asterisk*. *B*, selective one-dimensional NOESY spectra of the same sample showing NOEs from proton H-3 of HQNO (*upper* spectrum) and from the OCH_3 groups of Q_1 (*lower* spectrum). Areas of interest are indicated by *dashed rectangles*. *C*, a plausible arrangement of the two ligands, Q_1 and HQNO, according to observed ILOEs is presented. Strong, medium, and weak ILOEs are depicted with *black*, *gray*, and *dashed gray arrows*, respectively.

Feng *et al.* (35) localized two ubiquinone-4 molecules in the binding site of Ndi1. One Q_4 is located close to FAD, and the other appears to be only loosely bound. This scenario might be very close to the situation of the Na^+-NQR characterized here.

It is noteworthy, however, that almost simultaneously Iwata *et al.* (36) published a structure of Ndi1 with only one Q_2 mol-

ecule in the binding site bound in a rather different way as compared with the study of Feng *et al.* (35). This controversy awaits clarification by independent experimental methods, *e.g.* NMR.

Here we show that the NqrA subunit of the Na^+-NQR binds two quinone-type ligands adjacent to each other in an extended binding site. We used the quinone analog and antagonist DBMIB, a well known inhibitor of electron transfer complexes, to serve as a second quinone-type ligand that can easily be distinguished from Q_1 by NMR spectroscopy. In addition, we found very similar results with another well known inhibitor, namely HQNO, which had been proposed to interact with Q-sites in earlier studies (19). Extension of our detailed NMR and kinetic studies to Q_2 as a ligand was unsuccessful probably because of unfavorable kinetics and interference caused by the detergent DDM (32).

In the current study, we provide (to our knowledge for the first time in the case of quinone-binding enzymes) direct experimental evidence that two quinone analog molecules are situated in immediate vicinity to each other in the binding pocket of NqrA. This result was obtained by measuring ILOEs between ubiquinone-1 and the inhibitors DBMIB and HQNO, respectively. NOEs between both molecules could in principle derive from several situations. If Q_1 and DBMIB or HQNO formed stable complexes in solution one would expect intermolecular NOEs. However, in the absence of NqrA, we did not detect intermolecular NOEs (see control experiment shown in Figs. 8 and 9). Alternatively, NOEs between Q_1 and inhibitors could have been mediated by protons of the binding site of NqrA. Such intermolecular NOEs, called INPHARMA effects, could build up even in a purely competitive binding situation (37). However, for INPHARMA effects to develop, it is relevant that the magnetization has to be "stored" on the receptor during the ligand exchange process. This transfer is not possible if the experiment is carried out with a perdeuterated receptor, and thus, INPHARMA effects should be absent or at least strongly reduced under these conditions. We performed the same experiment with protonated as well as perdeuterated NqrA (^2H labeling $\geq$95% according to mass spectrometry) and saw no significant reduction in the intensity of the ILOE cross-peaks (Fig. 8). The only plausible interpretation is simultaneous binding of both ligands directly adjacent to each other within an extended quinone binding site of NqrA.

In the case of DBMIB, the precise relative arrangement of Q_1 and DBMIB within the binding site cannot be determined to great accuracy from the ILOEs because of the generally low signal intensity and because essentially all protons of Q_1 show ILOEs to all protons of DBMIB with slightly varying intensities. Interestingly, in the case of HQNO, the strongest ILOEs toward protons of Q_1 originate from protons located at the terminus of the aliphatic chain, suggesting that the alkyl chain of HQNO is oriented toward Q_1 during simultaneous binding to NqrA (Fig. 9*A*). Furthermore, we could exploit the high sensitivity of selective one-dimensional double pulsed field gradient spin-echo NOESY experiments to show that H-3 is the only aromatic proton of HQNO that displays a weak ILOE effect to the methoxy groups of Q_1 (Fig. 9*B*). Taking all observed (and absent) ILOEs into account, we propose a plausible arrangement of the two ligands, Q_1 and HQNO, adopted during simultaneous binding to the NqrA subunit (Fig. 9*C*), noting, however, that this should not be considered as a unique solution.

The fact that DBMIB does not displace Q_1 from the binding site in a competitive manner is furthermore supported by an STD NMR titration. In a competitive binding situation, the STD effects of Q_1 should decrease upon titrating in DBMIB because DBMIB would displace Q_1 from the binding site, lowering the fraction of bound Q_1 and, thus, lowering the amount of saturation transferred from NqrA to Q_1. However, we observed exactly the opposite. Increasing the concentration of DBMIB led to a markedly increasing STD effect of Q_1. In addition, in the presence of DBMIB, the ratio of STD effects of individual protons differed from the situation without inhibitor. This suggests that DBMIB alters the binding mode of Q_1, which in turn leads to a more efficient saturation transfer and therefore stronger STD effects. The EC_{50} of this interaction was 27 μM. A similar effect was observed in the case of HQNO with an EC_{50} of 51 μM. This finding, in addition to the presence of ILOEs between Q_1 and both DBMIB and HQNO, respectively, suggests that simultaneous binding of quinone analog ligands could be a general mechanism.

Our current results show that DBMIB, at the accessible concentration of 400 μM, is not able to displace Q_1 from the binding site as we saw the highest STD effects of Q_1 at this concentration of DBMIB. Also the presence of substantial ILOEs under these conditions indicates that apparently the "mixed situation" with 1 eq of Q_1 and 1 eq of DBMIB residing at the same time in the binding site is favored over double occupancy by 2 eq of DBMIB. However, the two-dimensional NOESY experiments provide evidence for double occupancy of two Q_1 molecules within the extended binding site of NqrA. Rather strong NOE correlations were observed between methyl groups of the isoprenyl chain of Q_1 and the methoxy groups of Q_1. Within the same Q_1, these protons are separated by 8–10 Å. Therefore, it is unlikely that these correlations originate from intramolecular dipolar interactions. Thus, we propose that these NOE contacts are indeed ILOEs between two individual Q_1 molecules. The fact that these cross-peaks showed up in the presence of protonated as well as deuterated NqrA further supports that these are true ILOEs and not due to relay or spin diffusion effects mediated by the protein.

Can these results, obtained with the isolated NqrA subunit, be transferred to the holo-Na^+-NQR complex? To gain insight into the physiological relevance, we performed the same STD NMR titration described above with Q_1 and DBMIB in the presence of holo-Na^+-NQR. This experiment provided an EC_{50} value of 28.5 μM, which is virtually identical to the EC_{50} value for NqrA.

To further confirm this result, we performed an enzyme inhibition experiment with the entire enzyme complex. In the presence of DBMIB, the rate of NADH oxidation (V_{max}) was decreased, whereas K_m was lowered. This is characteristic of an uncompetitive mode of inhibition typical for multisubstrate enzymes. That the catalytic site of NADH oxidation was not perturbed by DBMIB is indicated by the fact that the ratios of V_{max} to K_m in the presence or absence of DBMIB remain constant (Table 1). First, this confirms the notion that DBMIB dis-

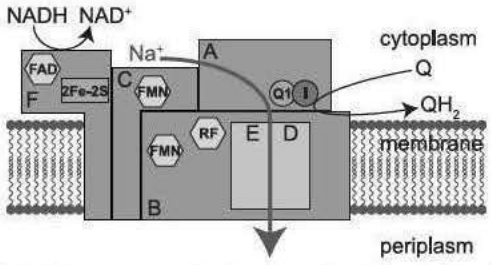

FIGURE 10. **Putative scheme of subunits and cofactors of the Na^+-NQR.** The Na^+-NQR is composed of one copy of each of its NqrA, -B, -C, -D, -E, and -F (*A–F*) subunits. NADH oxidation triggers reduction of FAD, a 2Fe-2S cluster, two FMNs, and a riboflavin within the complex. Two quinone analog ligands are predicted to interact within an extended Q binding site located on the NqrA subunit; in the current work, these are Q_1 and an inhibitor (*I*) (DBMIB or HQNO, respectively). The final electron transfer step during catalysis by the Na^+-NQR occurs from riboflavin (*RF*) on the NqrB subunit (*B*) to quinone on NqrA.

rupts the electron pathway further downstream, presumably at the quinone reductase site due to the structural resemblance to ubiquinone (Fig. 1). Second, this ascertains that NADH oxidase and quinone reductase sites of the Na^+-NQR are coupled in our experimental setup and no electrons short circuit to quinone at the level of the NADH oxidase. This needs to be considered because Q_1 can serve as an artificial electron acceptor when assaying the isolated NADH dehydrogenase domain (38). For quinone reduction, we observed a mixed mode of inhibition in the presence of DBMIB as documented by the rates of quinol formation.

Evaluating our experiments according to a Michaelis-Menten model yielded an average inhibition constant (K_I') of 53.2 μM. This K_I value is strikingly similar to the EC_{50} values determined in the STD NMR experiments with the NqrA subunit and the holo-Na^+-NQR complex (26.7 $\pm$ 2.6 and 28.5 $\pm$ 11.2 μM, respectively). In summary, this strongly indicates that the interaction of the inhibitor DBMIB with the extended binding site of the NqrA subunit is causing the inhibition of enzymatic turnover measured with the holoenzyme complex.

Recently, Juárez *et al.* (10) investigated in *V. cholerae* Na^+-NQR two mutations that had been discovered earlier in the Na^+-NQR of *V. alginolyticus*. These mutations in subunit NqrB confer resistance to the antibiotic korormicin in *V. alginolyticus* (8). Mutations of glycine residues Gly-140 and Gly-141, located in the NqrB subunit, to alanines were found to have a profound effect on the enzymatic activity of Na^+-NQR, leading the authors to propose that the NqrB subunit carries the site of quinone reduction (10). Our current study supports our earlier results indicating that the NqrA subunit carries the catalytically relevant quinone binding site of the Na^+-NQR. One should consider that long range structural perturbations induced by mutations on subunit NqrB might affect the quinone binding properties of subunit NqrA.

A plausible extension of our results shown here is to assume that holo-Na^+-NQR also binds 2 eq of the natural substrate, Q_8, with their hydrophilic headgroups *in vivo*. We propose that these two quinones are central to the last electron transfer steps. In this model, two subsequent one-electron transfers, probably from a flavosemiquinone located on the NqrB subunit, would reduce ubiquinone to the ubisemiquinone and subsequently to ubiquinol, which is then released by the enzyme. A schematic view of the Na^+-NQR complex with the two binding sites for quinones and quinone analogs located on the NqrA subunit is shown in Fig. 10.

The presence of two quinones in the binding site could enhance the efficiency of catalysis in at least two ways. One quinone ligand could serve essentially as a cofactor that remains tightly bound to the enzyme and switches between the quinone and the semiquinone state, whereas the other quinone ligand is much less tightly bound, reduced in two steps to the quinol, and then released from the enzyme. Alternatively, the second, low affinity binding site could constitute a waiting position for the next ubiquinone substrate to enter the site of reduction, leading to a faster supply of fresh substrate and, thus, accelerated enzymatic turnover. Which of these mechanisms is finally operational in the Na^+-NQR will be addressed in future studies.

Acknowledgment—We are grateful to Susan Kyncl for critically reading the manuscript.

REFERENCES

1. Häse, C. C., and Barquera, B. (2001) Role of sodium bioenergetics in *Vibrio cholerae*. *Biochim. Biophys. Acta* **1505,** 169–178
2. Barquera, B., Ramirez-Silva, L., Morgan, J. E., and Nilges, M. J. (2006) A new flavin radical signal in the Na^+-pumping NADH:quinone oxidoreductase from *Vibrio cholerae*: an EPR/electron nuclear double resonance investigation of the role of the covalently bound flavins in subunits B and C. *J. Biol. Chem.* **281,** 36482–36491
3. Tao, M., Casutt, M. S., Fritz, G., and Steuber, J. (2008) Oxidant-induced formation of a neutral flavosemiquinone in the Na^+-translocating NADH:quinone oxidoreductase (Na^+-NQR) from *Vibrio cholerae*. *Biochim. Biophys. Acta* **1777,** 696–702
4. Casutt, M. S., Huber, T., Brunisholz, R., Tao, M., Fritz, G., and Steuber, J. (2010) Localization and function of the membrane-bound riboflavin in the Na^+-translocating NADH:quinone oxidoreductase (Na^+-NQR) from *Vibrio cholerae*. *J. Biol. Chem.* **285,** 27088–27099
5. Bogachev, A. V., Bloch, D. A., Bertsova, Y. V., and Verkhovsky, M. I. (2009) Redox properties of the prosthetic groups of Na^+-translocating NADH:quinone oxidoreductase. 2. Study of the enzyme by optical spectroscopy. *Biochemistry* **48,** 6299–6304
6. Juárez, O., Morgan, J. E., and Barquera, B. (2009) The electron transfer pathway of the Na^+-pumping NADH:quinone oxidoreductase from *Vibrio cholerae*. *J. Biol. Chem.* **284,** 8963–8972
7. Juárez, O., Morgan, J. E., Nilges, M. J., and Barquera, B. (2010) Energy transducing redox steps of the Na^+-pumping NADH:quinone oxidoreductase from *Vibrio cholerae*. *Proc. Natl. Acad. Sci. U.S.A.* **107,** 12505–12510
8. Hayashi, M., Shibata, N., Nakayama, Y., Yoshikawa, K., and Unemoto, T. (2002) Korormicin insensitivity in *Vibrio alginolyticus* is correlated with a single point mutation of Gly-140 in the NqrB subunit of the Na^+-translocating NADH-quinone reductase. *Arch. Biochem. Biophys.* **401,** 173–177
9. Casutt, M. S., Nedielkov, R., Wendelspiess, S., Vossler, S., Gerken, U., Murai, M., Miyoshi, H., Möller, H. M., and Steuber, J. (2011) Localization of ubiquinone-8 in the Na^+-pumping NADH:quinone oxidoreductase from *Vibrio cholerae*. *J. Biol. Chem.* **286,** 40075–40082
10. Juárez, O., Neehaul, Y., Turk, E., Chahboun, N., DeMicco, J. M., Hellwig, P., and Barquera, B. (2012) The role of glycine residues 140 and 141 of subunit B in the functional ubiquinone binding site of the Na^+-pumping NADH:quinone oxidoreductase from *Vibrio cholerae*. *J. Biol. Chem.* **287,** 25678–25685
11. Chain, R. K., and Malkin, R. (1979) On the interaction of 2,5-dibromo-3-methyl-6-isopropylbenzoquinone (DBMIB) with bound electron carriers in spinach chloroplasts. *Arch. Biochem. Biophys.* **197,** 52–56

12. Degli Esposti, M., Rugolo, M., and Lenaz, G. (1983) Inhibition of the mitochondrial bc1 complex by d bromothymoquinone. *FEBS Lett.* **156,** 15–19
13. Draber, W., Trebst, A., and Harth, E. (1970) On a new inhibitor of photosynthetic electron-transport in isolated chloroplasts. *Z. Naturforsch. B* **25,** 1157–1159
14. Loschen, G., and Azzi, A. (1974) Dibromothymoquinone: a new inhibitor of mitochondrial electron transport at the level of ubiquinone. *FEBS Lett.* **41,** 115–117
15. Rich, P. R. (1984) Electron and proton transfers through quinones and cytochrome bc complexes. *Biochim. Biophys. Acta* **768,** 53–79
16. Simkovic, M., and Frerman, F. E. (2004) Alternative quinone substrates and inhibitors of human electron-transfer flavoprotein-ubiquinone oxidoreductase. *Biochem. J.* **378,** 633–640
17. Roberts, A. G., Bowman, M. K., and Kramer, D. M. (2004) The inhibitor DBMIB provides insight into the functional architecture of the Qo site in the cytochrome b6f complex. *Biochemistry* **43,** 7707–7716
18. Degli Esposti, M., Rotilio, G., and Lenaz, G. (1984) Effects of dibromothymoquinone on the structure and function of the mitochondrial bc1 complex. *Biochim. Biophys. Acta* **767,** 10–20
19. Pfenninger-Li, X. D., Albracht, S. P., van Belzen, R., and Dimroth, P. (1996) NADH:ubiquinone oxidoreductase of *Vibrio alginolyticus*: purification, properties, and reconstitution of the Na^+ pump. *Biochemistry* **35,** 6233–6242
20. Ding, H., Moser, C. C., Robertson, D. E., Tokito, M. K., Daldal, F., and Dutton, P. L. (1995) Ubiquinone pair in the Qo site central to the primary energy conversion reactions of cytochrome bc1 complex. *Biochemistry* **34,** 15979–15996
21. Bartoschek, S., Johansson, M., Geierstanger, B. H., Okun, J. G., Lancaster, C. R., Humpfer, E., Yu, L., Yu, C. A., Griesinger, C., and Brandt, U. (2001) Three molecules of ubiquinone bind specifically to mitochondrial cytochrome bc1 complex. *J. Biol. Chem.* **276,** 35231–35234
22. Roberts, A. G., and Kramer, D. M. (2001) Inhibitor "double occupancy" in the Q_o pocket of the chloroplast cytochrome b_6f complex. *Biochemistry* **40,** 13407–13412
23. Casutt, M. S., Wendelspiess, S., Steuber, J., and Fritz, G. (2010) Crystallization of the Na^+-translocating NADH:quinone oxidoreductase from *Vibrio cholerae*. *Acta Crystallogr. Sect. F Struct. Biol. Cryst. Commun.* **66,** 1677–1679
24. Marley, J., Lu, M., and Bracken, C. (2001) A method for efficient isotopic labeling of recombinant proteins. *J. Biomol. NMR* **20,** 71–75
25. Voet, D., and Voet, J. G. (2011) *Biochemistry*, 4th Ed., pp. 482–506, Wiley, Hoboken, NJ
26. Mayer, M., and Meyer, B. (1999) Characterization of ligand binding by saturation transfer difference NMR spectroscopy. *Angew. Chem. Int. Ed. Engl.* **38,** 1784–1788
27. Hwang, T. L., and Shaka, A. J. (1995) Water suppression that works—excitation sculpting using arbitrary wave forms and pulsed field gradients. *J. Magn. Reson. Ser. A* **112,** 275–279
28. Hoult, D. I. (1976) Solvent peak saturation with single phase and quadrature Fourier transformation. *J. Magn. Reson.* **21,** 337–347
29. Hore, P. J. (1989) Solvent suppression. *Methods Enzymol.* **176,** 64–77
30. Stonehouse, J., Adell, P., Keeler, J., and Shaka, A. J. (1994) Ultrahigh-quality NOE spectra. *J. Am. Chem. Soc.* **116,** 6037–6038
31. Lin, P. C., Türk, K., Häse, C. C., Fritz, G., and Steuber, J. (2007) Quinone reduction by the Na^+-translocating NADH dehydrogenase promotes extracellular superoxide production in *Vibrio cholerae*. *J. Bacteriol.* **189,** 3902–3908
32. Lenaz, G. (1998) Quinone specificity of complex I. *Biochim. Biophys. Acta* **1364,** 207–221
33. Li, D., DeRose, E. F., and London, R. E. (1999) The inter-ligand Overhauser effect: a powerful new NMR approach for mapping structural relationships of macromolecular ligands. *J. Biomol. NMR* **15,** 71–76
34. Nakayama, Y., Hayashi, M., Yoshikawa, K., Mochida, K., and Unemoto, T. (1999) Inhibitor studies of a new antibiotic, korormicin, 2-n-heptyl-4-hydroxyquinoline N-oxide and Ag^+ toward the Na^+-translocating NADH-quinone reductase from the marine *Vibrio alginolyticus*. *Biol. Pharm. Bull.* **22,** 1064–1067
35. Feng, Y., Li, W., Li, J., Wang, J., Ge, J., Xu, D., Liu, Y., Wu, K., Zeng, Q., Wu, J. W., Tian, C., Zhou, B., and Yang, M. (2012) Structural insight into the type-II mitochondrial NADH dehydrogenases. *Nature* **491,** 478–482
36. Iwata, M., Lee, Y., Yamashita, T., Yagi, T., Iwata, S., Cameron, A. D., and Maher, M. J. (2012) The structure of the yeast NADH dehydrogenase (Ndi1) reveals overlapping binding sites for water- and lipid-soluble substrates. *Proc. Natl. Acad. Sci. U.S.A.* **109,** 15247–15252
37. Sánchez-Pedregal, V. M., Reese, M., Meiler, J., Blommers, M. J., Griesinger, C., and Carlomagno, T. (2005) The INPHARMA method: protein-mediated interligand NOEs for pharmacophore mapping. *Angew. Chem. Int. Ed. Engl.* **44,** 4172–4175
38. Türk, K., Puhar, A., Neese, F., Bill, E., Fritz, G., and Steuber, J. (2004) NADH oxidation by the Na^+-translocating NADH:quinone oxidoreductase from *Vibrio cholerae*: functional role of the NqrF subunit. *J. Biol. Chem.* **279,** 21349–21355